

PoseBH: Prototypical Multi-Dataset Training Beyond Human Pose Estimation

Uyoung Jeong¹ Jonathan Freer² Seungryul Baek¹ Hyung Jin Chang² Kwang In Kim³

¹UNIST ²University of Birmingham ³POSTECH

Abstract

We study multi-dataset training (MDT) for pose estimation, where skeletal heterogeneity presents a unique challenge that existing methods have yet to address. In traditional domains, e.g. regression and classification, MDT typically relies on dataset merging or multi-head supervision. However, the diversity of skeleton types and limited cross-dataset supervision complicate integration in pose estimation. To address these challenges, we introduce PoseBH, a new MDT framework that tackles keypoint heterogeneity and limited supervision through two key techniques. First, we propose nonparametric keypoint prototypes that learn within a unified embedding space, enabling seamless integration across skeleton types. Second, we develop a cross-type self-supervision mechanism that aligns keypoint predictions with keypoint embedding prototypes, providing supervision without relying on teacher-student models or additional augmentations. PoseBH substantially improves generalization across whole-body and animal pose datasets, including COCO-WholeBody, AP-10K, and APT-36K, while preserving performance on standard human pose benchmarks (COCO, MPII, and AIC). Furthermore, our learned keypoint embeddings transfer effectively to hand shape estimation (InterHand2.6M) and human body shape estimation (3DPW). The code for PoseBH is available at: <https://github.com/uyoung-jeong/PoseBH>.

1. Introduction

The demand for human pose estimators has grown substantially in recent years, driving their adoption across diverse applications, including 3D avatar generation [15, 26, 32], motion generation [16, 23, 34], human-robot interaction [21, 46, 63], safety monitoring [7, 19, 41], and VR/AR tracking [13, 45, 49]. These domains pose distinct operational challenges, often necessitating significant domain adaptation for robust pose estimation. To address this, we aim to train a human pose estimator that generalizes effectively across multiple datasets.

However, multi-dataset training (MDT) for pose estimation presents two key challenges. First, keypoints

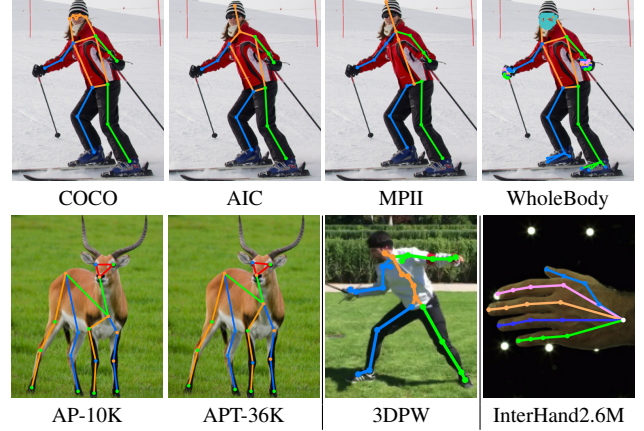


Figure 1. PoseBH unifies diverse skeleton formats, including humans, hands, and animals. The displayed skeletons show pose estimation results from our method, with 3DPW and InterHand2.6M predictions from a transferred model.

are heterogeneous across different datasets. For example, COCO [24] and MPII [1] define 17 and 16 keypoints, respectively, with 9 non-overlapping ones. Even when datasets share keypoints with identical names, their localization characteristics often differ due to domain gaps. For example, while COCO and animal datasets (e.g., AP-10K [62] and APT-36K [60]) use common keypoint names such as eyes, nose, and hips, significant anatomical differences exist (see Fig. 1). As a result, naively merging the identically named keypoints is ineffective.

Second, pose estimation MDT suffers from a lack of adequate supervision. In MDT, multiple skeleton types from different datasets are trained for each input instance. However, only a single skeleton-type ground truth is provided per input, leaving others unsupervised. This limitation resembles a semi-supervised learning challenge, constraining performance on smaller datasets. Existing semi-supervised learning methods typically rely on input augmentation or teacher-student knowledge distillation, both of which require substantial extra computational overhead.

Existing approaches fail to fully address these challenges, often relying on a shared backbone network [6] or

a mixture of experts [56] to preserve downstream performance. However, these methods tend to focus on mainstream datasets like COCO or MPII, resulting in degraded performance on underrepresented datasets. We propose a method that enhances performance in discrepant domains while maintaining accuracy on standard human pose datasets. A straightforward fine-tuning approach on the target domain often disrupts performance on source datasets, as it fails to balance differences in skeleton structures and dataset distributions. Therefore, effective generalization requires jointly harmonizing skeletal representations and dataset diversity during training.

We achieve this through two primary techniques. First, we introduce prototypes to represent keypoints as embedding vectors, providing a unified representation across datasets. We regress pixel-wise keypoint embeddings from backbone features and match them to corresponding prototypes, automating keypoint mapping across datasets. This enables the integration of diverse keypoint types, including whole-body and animal keypoints, despite significant skeletal differences. Furthermore, our keypoint prototypes are non-learnable parameters, offering adaptability and computational efficiency for domain transfer.

Second, we generate reliable self-supervision signals using the predicted keypoints and their embeddings, a process we term *cross-type self-supervision*. Since keypoint predictions can be obtained via a dot product between embeddings and prototypes, we effectively establish two distinct keypoint prediction modalities. By aligning these predictions, we filter out noisy keypoints and produce reliable labels for supervising unlabeled keypoints. This process enhances the utility of embeddings without requiring additional networks or input augmentation. As a result, we provide effective supervision for underrepresented and discrepant datasets, achieving a higher degree of generalizability.

Our main technical contributions are as follows:

- Keypoint prototypes for learning arbitrary keypoints from multiple datasets ensuring high transferability.
- A cross-type self-supervision mechanism that aligns keypoint regression outputs with keypoint embeddings, enriching supervision for unlabeled keypoints.
- Strong generalization across estimation tasks, including whole-body, animal, and hand pose estimation, as well as human shape estimation.

2. Related works

Multi-dataset training has been widely explored in various computer vision tasks. Relabeling and pseudo-labeling are among the most straightforward yet resource-intensive approaches. For example, MSeg [20] employed relabeling for segmentation, while [68] used offline pseudo-labeling for object detection. However, both methods face scalability challenges, as adding a new dataset requires reprocessing

annotations for all previously processed datasets to redefine the class set, leading to a quadratic computational cost.

Several approaches have been proposed to improve scalability. In object detection, [4, 70] aim to unify object class labels by merging similar categories. However, they struggle to integrate localization features of the same object due to the absence of spatial information in class logits. UniTrack learns a unified identity embedding through self-supervised learning for multiple object-tracking tasks, including human pose tracking [51]. However, it prioritizes pose propagation over estimation and relies exclusively on the PoseTrack18 [2] skeleton, without incorporating multiple pose datasets.

Another class of methods [50, 54, 58, 66] employs network modules, such as graph convolutional networks (GCN), for cross-dataset adaptation. However, these dataset-specific modules limit domain transferability, as their input and output sizes are dictated by the label structure, making them incompatible with datasets that have different keypoint formats. In contrast, our approach achieves flexible transferability without relying on dataset-specific domain adaptation modules.

Human pose estimation with MDT. In 3D human shape estimation, several methods have used pseudo-ground truths (GTs) generated by the SMPL model for MDT [5, 18, 43, 44]. However, these pseudo-GTs are often inaccurate due to depth ambiguity in 2D images and the limited expressiveness of the parametric 3D model [30, 31]. Similar to [70], Sáráandi et al.’s affine-combining autoencoder (ACAE) merges 3D joint coordinates via an autoencoder [37]. However, the autoencoder’s learnable parameters are dataset-dependent, limiting its generalizability. Furthermore, ACAE does not preserve pixel-level features, making it unsuitable when spatial information is crucial.

Recent works on category-agnostic pose estimation integrate various objects, such as chairs and vehicles, by combining multiple datasets [14, 55]. These methods follow a relabeling approach, creating a superset of keypoint classes and detecting only the keypoints defined in their relabeled dataset. As a result, they do not address keypoint heterogeneity or label sparsity issues, as training and evaluation occur within a single labeled dataset. In contrast, our method uses multiple skeletons to improve generalization across diverse downstream domains.

In 2D human pose estimation, UniHCP performs multiple human perception tasks using task-specific queries without incorporating task-specific layers inside the backbone [6]. This design limits its ability to generalize to distant domains such as animals and whole-body pose estimation. ViTPose++ [56] and Sapiens [17] employ multi-head architectures for MDT but do not address skeleton heterogeneity or the resulting label sparsity.

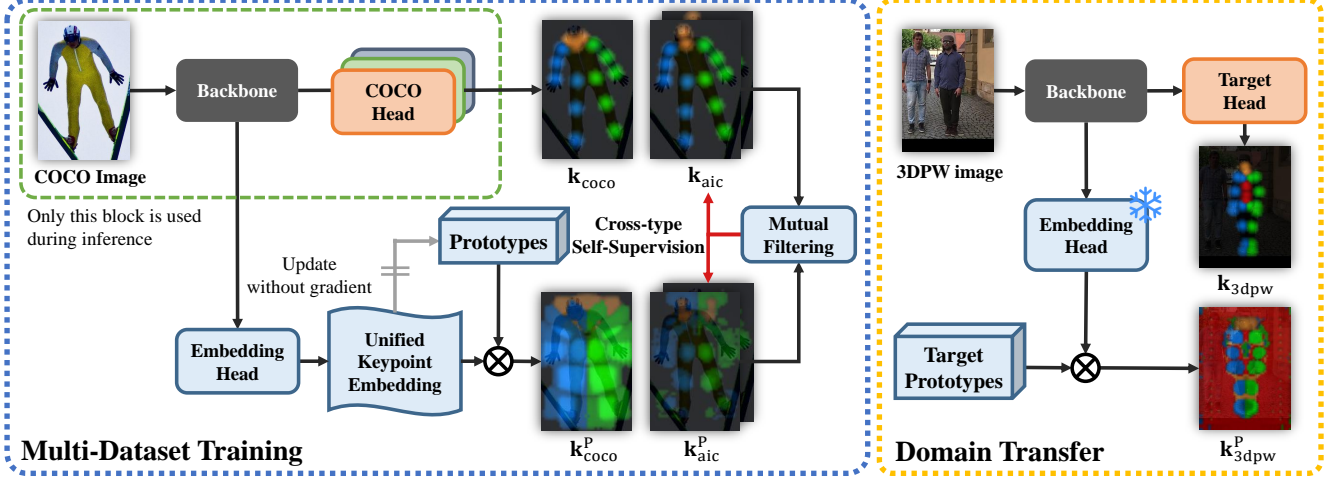


Figure 2. Overview of the PoseBH architecture. During training, the embedding head maps the backbone features into a unified keypoint embedding space. By matching these embeddings with prototypes, dataset-specific keypoint heatmaps $\mathbf{k}_{\text{coco}}^p$ are generated. Prototypes are updated nonparametrically from the embeddings. During inference, the embedding head and the subsequent procedures are removed.

Prototype learning can be interpreted as proxy-based metric learning [36], where the centers of a fixed set of clusters serve as prototypes. This approach has been studied in various domains, including semantic segmentation [8, 10, 69], person re-identification [33], meta-learning [25, 40, 61, 65], and visual interpretability [3, 9, 48].

ProtoSeg [69] introduces a nonparametric approach to semantic segmentation by assigning multiple prototypes per class. ProMotion [28] employs prototypes to unify scene depth estimation and optical flow tasks. While our method draws inspiration from ProtoSeg and aligns with ProMotion in exploiting the benefits of prototypes for MDT, it differs in three key aspects. First, our approach applies keypoint-level supervision, which is inherently sparser than segmentation, depth, or optical flow. Second, we specifically address skeleton heterogeneity and cross-dataset relationships, aspects not considered by ProtoSeg and ProMotion. Third, while ProtoSeg and ProMotion apply fully supervised learning, our method tackles the challenge of unlabeled data, a problem unique to MDT pose estimation.

3. Method

We focus on multi-dataset training (MDT) for 2D human pose estimation. Given D datasets, our model predicts a keypoint heatmap for a person, represented as an array $\mathbf{k}_d \in \mathbb{R}^{J_d \times H \times W}$, where d is the dataset index, J_d is the number of keypoints in the d -th dataset, and H and W denote the height and width of the heatmap, respectively.

3.1. Multi-head baseline

The multi-head baseline model consists of a backbone network that extracts an output backbone feature map from

an input RGB image. The backbone network is shared across all datasets, while individual keypoint heads independently regress dataset-wise keypoint heatmaps $\{\mathbf{k}_d\}_{d=1}^D$, each trained with its corresponding labels. The keypoint heads share the same architecture, except for the final layer, where the output channel size is the respective number of keypoints. This generic baseline does not share the keypoint output space, limiting the MDT effect up to the backbone.

3.2. Keypoint prototype learning

Overview. Our goal is to learn a unified keypoint space that standardizes keypoint output formats across datasets, scales with dataset size, and retains dataset-specific localization accuracy. To achieve this, we reformulate keypoint regression as a prototype-based distance metric learning problem (see Fig. 2). Our shared keypoint embedding module generates a normalized keypoint embedding map $\mathbf{e} \in \mathbb{R}^{F \times H \times W}$ from an input feature map. The module consists of two deconvolution layers, followed by a residual block and two convolution layers. Additional details are provided in the supplementary document.

Using embeddings and prototypes, we perform keypoint classification by matching embeddings with prototypes $\mathbf{P} \in \mathbb{R}^{J \times M \times F}$, where F is the embedding dimension, J is the total number of keypoints across all datasets, M is the number of in-class prototypes. For each heatmap pixel, we compute the cosine similarity between the prototypes and the embedding vector to obtain keypoint predictions:

$$\mathbf{k}_{j,y,x}^p = \max_m \frac{\mathbf{P}_{(j,m,:)} \cdot \mathbf{e}_{(:,y,x)}}{\|\mathbf{P}_{(j,m,:)}\| \|\mathbf{e}_{(:,y,x)}\|}, \quad (1)$$

where x, y denote pixel indices in the heatmap, and $\mathbf{P}_{(j,m,:)}$ is a row vector of size F , extracted $\mathbf{P} \in \mathbb{R}^{J \times M \times F}$ along its

first two dimensions. For each keypoint class j , $\mathbf{k}_{(j,:,:) }^P \in \mathbb{R}^{H \times W}$ stores the matching score of the most probable prototype among M prototypes. We refer to this as the *prototype keypoint heatmap* \mathbf{k}^P to distinguish it from the multi-head outputs \mathbf{k} .

For the remainder of this paper, we use the following notation: $\mathbf{A}_{(:, :, a)}$ denotes the 2D slice of a 3D array \mathbf{A} indexed at a along the third dimension, while $\mathbf{A}_{(:, b, :)}$ represents the 2D slice at index b along the second dimension. Similarly, $\mathbf{A}_{(d, e, :, :)}$ represents the 3D sub-array spanning indices d to e along the first dimension. For a 2D array \mathbf{B} , $\mathbf{B}_{(:, c)}$ indicates the c -th column vector, whereas $\mathbf{B}_{(d, c)}$ refers to the element at position (d, c) .

Prototype learning. We adopt a nonparametric learning approach [69] to train \mathbf{P} . First, we obtain logits $\{\mathbf{l}_j\}_{j=1}^J \subset \mathbb{R}^{M \times N}$ and targets $\{\mathbf{t}_j \in \mathbb{R}^{N_j}\}_{j=1}^J$, where N_j is the number of foreground samples (i.e., pixels in the ground-truth (GT) heatmap with nonzero values) for the j -th joint, and N is the total number of foreground samples across all joints. We define logits as sampled embedding vectors and targets as keypoint class labels, with each keypoint class selecting an in-class prototype from M candidates.

Since no GT selection is explicitly provided, we assign an in-class prototype for each logit via online clustering using Sinkhorn-Knopp iteration with an equipartition constraint [39], and compute \mathbf{t}_j as follows:

$$\mathbf{l}_j = \mathbf{P}_{(j, :, :)} \bar{\mathbf{e}}, \quad (2)$$

$$\mathbf{t}_j = \arg \max_m \text{diag}(\mathbf{u}) \exp \left(\frac{\mathbf{l}_j}{\kappa} \right) \text{diag}(\mathbf{v}), \quad (3)$$

where $\bar{\mathbf{e}}$ is a 2D array of size $F \times N_j$, obtained by first flattening $\mathbf{e} \in \mathbb{R}^{F \times H \times W}$ along the spatial dimensions into a 2D array of size $F \times (HW)$ and then, selecting N_j foreground objects. $\text{diag}(\mathbf{u})$ is a diagonal matrix derived from the vector \mathbf{u} , and $\exp(\cdot)$ is applied element-wise.

Each prototype is then updated with momentum λ :

$$\mathbf{P}_{j, m}^{\text{new}} = \lambda \mathbf{P}_{j, m}^{\text{old}} + (1 - \lambda) \frac{1}{N_j} \sum_{n=1}^{N_j} w_{mn} \bar{\mathbf{e}}_{(:, n)}, \quad (4)$$

where w_{mn} is the clustering assignment weight, calculated similarly to Eq. (3), but using max instead of arg max.

To optimize the learned embedding with respect to the prototype \mathbf{P} , we employ pixel-prototype contrastive learning, using the pixel-prototype contrastive loss (PPC) and pixel-prototype distance (PPD) from [69]:

$$\mathcal{L}_{\text{PPC}}(\mathbf{l}_j, \mathbf{t}_j) = \frac{c_n}{N_j} \sum_{n=1}^{N_j} \text{CE}(\mathbf{l}_{j, n}, \mathbf{t}_{j, n}), \quad (5)$$

$$\mathcal{L}_{\text{PPD}}(\mathbf{l}_j, \mathbf{t}_j) = \frac{c_n}{N_j} \sum_{n=1}^{N_j} (1 - \mathbf{l}_{j, n}^{m+})^2, \quad (6)$$

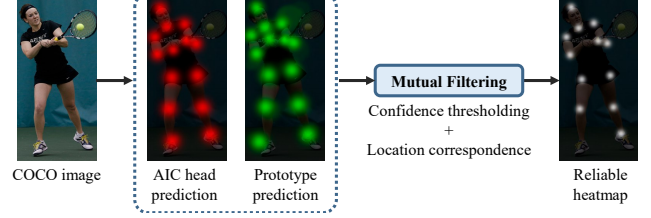


Figure 3. An illustrative example of cross-type self-supervision. Given a COCO image, we jointly refine the AIC head and AIC prototype predictions to produce reliable AIC heatmaps.

where c_n is the confidence value from the GT heatmap, CE denotes the cross-entropy loss, and m^+ indexes the first dimension of \mathbf{l}_d . For each dataset d , we collect logits $\mathbf{l}_{j, n} \in \mathbb{R}^{M \times N_d}$ and targets $\mathbf{t}_d \in \mathbb{R}^{N_d}$, where N_d is the number of samples in dataset d . The total prototype loss is then defined as $\mathcal{L}_{\text{Proto}} = \mathcal{L}_{\text{PPC}} + \mathcal{L}_{\text{PPD}}$.

Unlike standard contrastive learning, $\mathcal{L}_{\text{Proto}}$ operates within a single dataset and lacks the push term for differing dataset skeletons. To introduce cross-dataset negatives, we apply K-means clustering to all prototypes, forming K ($=96$) clusters. This clustering is performed only once during training, while online clustering for in-class prototypes is conducted at each iteration. These clusters serve as negative samples, where the embeddings closest to each centroid are used as logits, with their dataset-specific labels as targets. Finally, we obtain \mathbf{l}_c and \mathbf{t}_c for each cluster and apply Eqs. (5) and (6) to enable cross-dataset contrastive learning.

3.3. Cross-type self-supervision

While our keypoint prototypes enable unified MDT, label sparsity remains a challenge, as each image is annotated for only one dataset, limiting supervision. To address this semi-supervised learning problem, we introduce a self-supervision strategy that bridges keypoint heatmaps and embeddings. By collaboratively filtering out noisy predictions from both the keypoint and embedding heads, we generate reliable keypoint heatmaps for training (see Fig. 3).

To eliminate uncertain keypoint predictions, we apply two filtering conditions. First, for each keypoint class, the confidence scores of both the keypoint and embedding heads must exceed a threshold ($c_{thr} = 0.25$). Second, the root mean square distance between their predictions must be below a threshold ($d_{thr} = 2.1$).

The filtered predictions are then combined using a weighted average:

$$\hat{\mathbf{y}}_i = s_i \hat{\mathbf{y}}_i^{\text{kpt}} + (1 - s_i) \hat{\mathbf{y}}_i^{\text{emb}}, \quad (7)$$

where $s_i = c_i^{\text{kpt}} / (c_i^{\text{kpt}} + c_i^{\text{emb}})$, i is the keypoint index, and $\hat{\mathbf{y}}$ and c represent the keypoint prediction and confidence score from each head, respectively.

Method	GFLOPS	COCO	AIC	MPII	Avg.
UniHCP	18.9	76.8	32.6	90.9	66.8
ViTPose++	18.5	77.0	31.6	93.1	67.2
Ours	18.5	77.3	32.1	93.2	67.5

Table 1. Comparison of different multi-dataset training methods on general human pose benchmarks, with computational complexity measured in GFLOPS during the evaluation phase.

Method	AP-10K	APT-36K	COCO-W	Avg.
UniHCP	56.5	62.0	20.1	46.2
ViTPose++	74.1	76.0	57.1	69.1
Ours	75.0	87.2	57.9	73.4

Table 2. Comparison of multi-dataset training methods on whole-body and animal domains. COCO-W refers to COCO-WholeBody. The reported metrics are AP(%).

From $\hat{\mathbf{y}}$, we generate a *reliable heatmap* \mathbf{k}^{CSS} following the standard GT heatmap generation process. The loss for unlabeled samples is then computed as:

$$\mathcal{L}_{\text{CSS}} = \sum_{d=1}^D \zeta [\mathcal{L}_{\text{hm}}(\mathbf{k}_{d[\mathbf{u}]}, \mathbf{k}_{d[\mathbf{u}]}^{\text{CSS}}) + \mathcal{L}_{\text{Proto}}(\mathbf{e}_{[\mathbf{u}]}, \mathbf{k}_{d[\mathbf{u}]}^{\text{CSS}})], \quad (8)$$

where \mathbf{u} denotes the indices of the unlabeled samples. This cross-type self-supervision (CSS) loss enables self-distillation between the dataset-wise keypoint head and the prototype, mitigating supervision shortage without requiring a teacher model or input duplication.

The final training loss is defined as:

$$\mathcal{L}_{\text{MDT}} = \mathcal{L}_{\text{KPL}} + \mathcal{L}_{\text{CSS}}, \text{ where} \quad (9)$$

$$\mathcal{L}_{\text{KPL}} = \sum_{d=1}^D [\mathcal{L}_{\text{hm}}(\mathbf{k}_d, \mathbf{k}_d^{\text{gt}}) + \mathcal{L}_{\text{Proto}}(\mathbf{e}, \mathbf{k}_d, \mathbf{k}_d^{\text{gt}})], \quad (10)$$

and \mathcal{L}_{hm} is the standard JointMSE loss [42].

4. Experiments

4.1. Experimental setup

We follow the experimental setup of ViTPose++ [56], using six human pose datasets for training. (1) COCO consists of 57,000 training and 5,000 validation images, annotated with 17 keypoints [24]. (2) AICChallenger (AIC) contains 210,000 training and 30,000 validation images, annotated with 14 keypoints [52]. (3) MPII includes approximately 15,000 training, 2,729 validation, and 5,700 test images, with 16 keypoints [1]. (4) AP-10K is an animal pose dataset with approximately 7,000 training, 1,000 validation, and 2,000

test images [62]. (5) APT-36K, a video-based animal pose dataset, consists of about 25,000 training, 3,600 validation, and 7,000 test images [60]. Both AP-10K and APT-36K share the same skeletal format with 17 keypoints, largely following COCO. (6) COCO-WholeBody extends COCO with whole-body annotations covering 133 keypoints [52]. We follow standard evaluation protocols, using the average precision (AP) metric based on object keypoint similarity (OKS) for COCO, AIC, COCO-WholeBody, AP-10K, and APT-36K. For MPII, the percentage of correct keypoints (PCK) metric is used [1].

For the domain transfer experiments, we use InterHand2.6M [29] and 3DPW [47]. InterHand2.6M is a two-hand pose estimation dataset containing approximately 2.6M frames, annotated with 21 keypoints. We adopt the ViTPose++ configuration for frame sampling and dataset splits (training, validation, and test). For evaluation, we use PCK, AUC, and EPE, consistent with ViTPose++. 3DPW is an in-the-wild 3D human shape estimation dataset with 18,000 training and 26,000 test frames, annotated with 24 keypoints. We use COCO-style AP and AR as evaluation metrics. In both InterHand2.6M and 3DPW, the projected 2D keypoints are used as ground-truths.

Further details on the experimental setups, the impact of varying hyperparameters, and failure case analysis can be found in the supplemental document.

4.2. Implementation details

Our multi-head baseline model is ViTPose++ [56]. We use an input image size of 256×192 and apply a flip test in all cases. The model is trained for 100 epochs using the AdamW optimizer with a weight decay factor of 0.1 and a step learning rate scheduler with an initial learning rate of 0.001. The learning rate is reduced by a factor of 0.1 at the 50th and 90th epochs. We use four NVIDIA A100 GPUs for training with the ViT-H backbone and four NVIDIA A6000 GPUs for training with the ViT-B backbone.

We employ a scheduling strategy for both the losses and the learning rate. Initially, we freeze the multi-head model, updating only the embedding module and prototypes for 50 epochs. In the subsequent 40 epochs, we train the multi-heads and the embedding module while keeping the prototypes and the backbone frozen. Finally, during the last 10 epochs, we train the entire network except the prototypes. At this stage, we introduce cross-type self-supervision loss. This progressive optimization approach accelerates training compared to training the entire network from the outset.

4.3. Comparison with existing MDT methods

In Tab. 1, we evaluate the competitiveness of our method against existing MDT approaches. For a fair comparison, all methods use the ViT-Base backbone and are trained under our dataset configuration. While UniHCP performs

Method	Backbone	Datasets	COCO				MPII	
			(AP \uparrow)	(AP ⁵⁰ \uparrow)	(AP ⁷⁵ \uparrow)	(AR \uparrow)	(PCKh \uparrow)	(PCKh@0.1 \uparrow)
HRNet	HRNet-W48	1	75.1	90.6	82.2	80.4	90.3 [†]	33.1 [†]
HRFormer	HRFormer-B	1	75.6	90.8	82.8	80.8	-	-
SimCC	HRNet-W48	1	76.1	90.6	82.9	81.2	90.0	36.8
PCT [†]	Swin-B	1	77.7	91.2	84.7	82.1	92.5	-
PCT [†]	Swin-H	1	79.3	91.5	85.9	-	-	-
UniHCP	ViT-B	33	76.1	-	-	-	93.2 ^{††}	-
ViTPose++-B	ViT-B	6	77.0	73.4	84.0	82.6	92.8	39.1
ViTPose++-H	ViT-H	6	79.4	91.9	85.7	84.8	94.2	41.6
Ours	ViT-B	6	77.3	90.8	84.2	82.4	93.2	39.3
Ours	ViT-H	6	79.5	91.9	85.8	84.5	94.2	42.0

Table 3. Comparison with state-of-the-art methods on COCO and MPII. Methods with [†] uses 256 \times 256 input size. ^{††} indicates additional fine-tuning on each dataset.

well on AIC, it achieves the lowest scores on COCO and MPII, resulting in an average of 66.8. We hypothesize that UniHCP’s parameter-sharing strategy causes well-represented pose datasets to dominate, hindering its generalization across different skeleton structures. ViTPose++ serves as both a multi-head model and the baseline for our method. Our algorithm surpasses ViTPose++ by 0.3 in average score and outperforms it on individual datasets. Given that these benchmark scores are highly saturated and our method maintains the same computation complexity as ViTPose++ during inference, this improvement is significant.

To further assess generalization, we test our method on animal and whole-body pose estimation datasets. Table 2 shows that our method consistently improves performance, despite significant domain discrepancies. UniHCP lags behind with an average score of 27.2, likely due to its parameter sharing strategy, which does not address skeleton heterogeneity. Our method also surpasses ViTPose++ by an average score of 4.3, demonstrating superior generalization beyond human skeletons. Specifically, it achieves gains of 0.9 AP on AP-10K, 11.2 AP on APT-36K, and 0.8 AP on COCO-WholeBody. Unlike existing methods that compromise either mainstream performance or adaptation to distant domains, our approach enhances both synergistically.

4.4. Comparison to state-of-the-art methods

In Tab. 3, we compare our method with state-of-the-art (SOTA) approaches on the COCO and MPII benchmarks, using scores reported in the respective papers. We also evaluate our method against SOTA approaches designed for single datasets, including HRNet [42], HRFormer [64], SimCC [22], and PCT [12]. On the COCO validation set, our method ranks second with the ViT-B backbone and achieves SOTA performance with the ViT-H backbone, reaching 79.5 AP. On the MPII validation set, our ViT-B

Method	InterHand2.6M			3DPW	
	PCK \uparrow	AUC \uparrow	EPE \downarrow	AP \uparrow	AR \uparrow
UniHCP	98.5	87.0	3.72	57.9	61.8
ViTPose++	98.3	86.2	4.02	81.7	85.2
Ours	98.6	87.1	3.70	83.6	87.1

Table 4. Transfer results on hand (Interhand2.6M) and human shape (3DPW) domains.

model performs comparably to the fine-tuned UniHCP and surpasses the SOTA on the PCKh@0.1 metric by 0.4 PCKh. These results demonstrate that our method effectively balances adaptability to diverse domains while maintaining competitive performance on standard benchmarks, aligning with our primary objective of improving generalization beyond mainstream tasks.

4.5. Transfer to hands and human shapes

PoseBH has the capability to generalize its learned representations beyond the training dataset. We validate this through domain transfer experiments by fine-tuning the model separately on the InterHand2.6M and 3DPW datasets. InterHand2.6M is a two-hand pose estimation dataset containing 21 MANO keypoints [35], while 3DPW is an in-the-wild human shape estimation dataset with 24 SMPL keypoints [27].

During fine-tuning, we freeze the embedding module and nonparametrically learn the prototypes for the target datasets. After convergence, we fine-tune the backbone and head weights alongside the prototype loss. Freezing the embedding module ensures that the previously learned prototypes and those of the target dataset remain aligned within the same embedding space, preserving the learned repre-

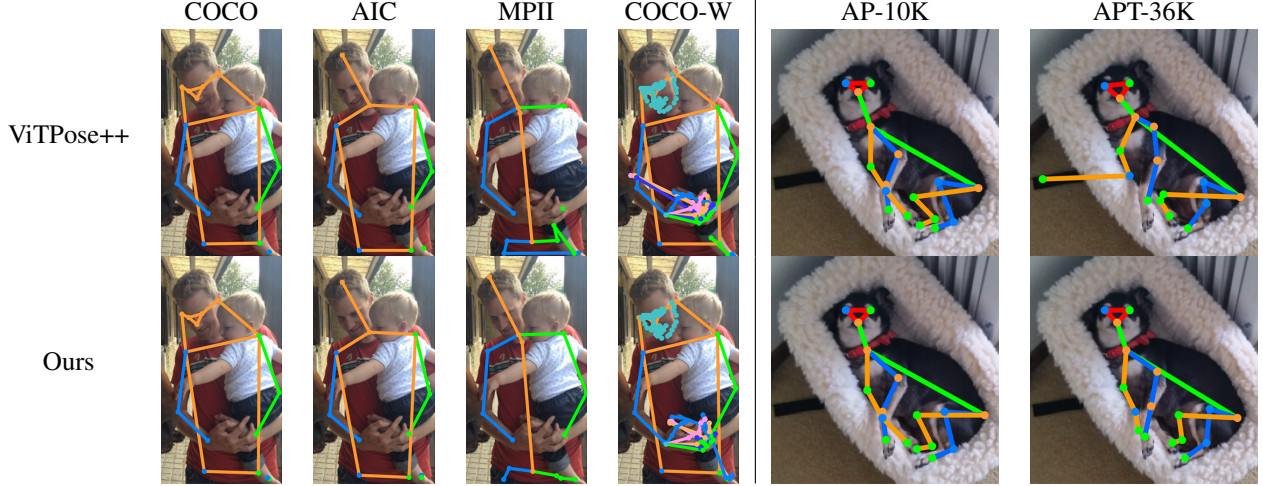


Figure 4. Comparative pose estimation results on human (left) and animal (dog; right).

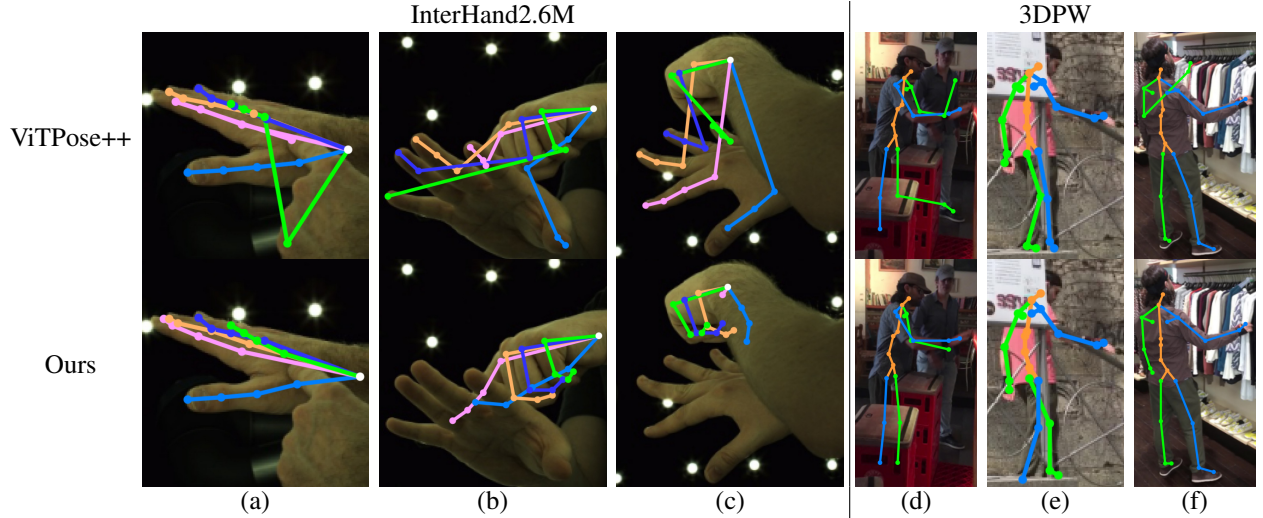


Figure 5. Comparative results on InterHand2.6M (a–c) and 3DPW (e–f).

sentations during transfer. Since these experiments do not involve skeleton heterogeneity across datasets, no semi-supervised learning challenges arise, and CSS loss is not applied.

In Tab. 4, we report results on the InterHand2.6M and 3DPW test sets using the ViT-B backbone. Given its large dataset size (~ 2.6 M instances), InterHand2.6M exhibits a smaller performance gap among different methods. Nonetheless, our method surpasses ViTPose++ by 0.3 PCK, 0.9 AUC, and 0.32 EPE, while also outperforming UniHCP by 0.1 PCK, 0.1 AUC, and 0.02 EPE. For the smaller 3DPW dataset, our method achieves a notable performance gain, surpassing the baseline by 1.9 AP and 1.9 AR, demonstrating strong generalization in keypoint embeddings.

4.6. Ablation studies

In Tab. 5, we present the results of ablation experiments on the COCO (CO), AIC (AI), MPII (MP), AP-10K (AP), APT-36K (APT), and COCO-Wholebody (CW) validation sets using the ViT-Base backbone. The top row represents a multi-head baseline with a shared backbone and dataset-specific heads. This conventional multi-head approach exhibits relatively low performance, particularly on the AP-10K and APT-36K validation sets, due to substantial domain discrepancies. Our keypoint prototype method achieves an average score of 66.3, improving the baseline by 0.8. Additionally, incorporating cross-type self-supervision provides an additional average performance gain of 0.2. Collectively, these enhancements enable our final configuration to outperform the multi-head baseline by an average of 2.4 points across all six datasets.

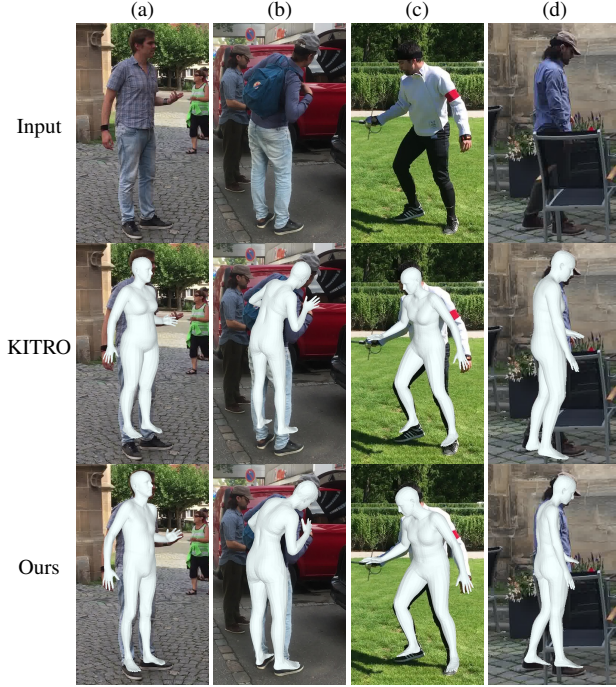


Figure 6. Examples of SMPL fitting using KITRO and with our 2D predictions.

Method	CO	AI	MP	AP	APT	CW	Avg.
Baseline	77.0	31.6	93.1	75.3	74.8	57.1	68.2
+ $\mathcal{L}_{\text{Proto}}$	77.0	31.8	93.0	76.4	86.4	57.5	70.4
+ \mathcal{L}_{CSS}	77.3	32.1	93.2	76.7	86.5	57.9	70.6

Table 5. Ablation study of the proposed method. $\mathcal{L}_{\text{Proto}}$: keypoint prototype learning. \mathcal{L}_{CSS} : cross-type self-supervision.

4.7. Visual analysis

Figure 4 presents examples of human and animal pose estimation, demonstrating that our algorithm achieves more accurate keypoint localization under complex interactions and occlusions, as seen in the right-hand keypoints of the standing person (left) and the right front toe of the dog (right).

We further compare the pose estimation results on InterHand2.6M and 3DPW in Fig. 5. In (a), ViTPose++ incorrectly assigns a little finger joint to the opposite hand, whereas our method provides more accurate localization. In (b), ViTPose++ struggles with occlusion from the other hand, producing noisy predictions, while our method correctly separates them. In (c), due to severe self-occlusion, ViTPose++ misestimates occluded keypoints and assigns them to the opposite hand, while our method generalizes well in challenging self-occlusion scenarios. In (d), ViTPose++ produces an implausible foot and hand pose under heavy occlusion, while our method remains robust. In

(e), ViTPose++ swaps the left and right legs, while our method correctly distinguishes them. In (f), background clutter causes ViTPose++ to produce noisy predictions for the left hand, while our method correctly identifies the location of the occluded left hand.

To further assess the effectiveness of our 2D SMPL keypoint predictions on the 3DPW test set, we employ a SMPL optimization technique. KITRO [59] optimizes SMPL parameters using 2D keypoint reprojection loss. For a comparative visual analysis, we replace KITRO’s 2D keypoint predictions with ours. As shown in Figure 6(a) and (c), KITRO fails to align the mesh with the actual feet, whereas our method achieves more precise alignment. In (b), KITRO mislocalizes the right hand under partial occlusion, while our 2D predictions remain robust. In (d), KITRO exhibits misalignment in both the hands and feet, while replacing its 2D predictions with ours significantly improves the alignment of peripheral body parts.

In the supplemental material, we provide a visualization of the prototypes generated by our algorithm, illustrating how they effectively capture the diversity of representations within the embedding space.

5. Conclusion

This paper presents a new multi-dataset training (MDT) framework for pose estimation across diverse domains and datasets. Traditional approaches encounter challenges with label heterogeneity, dataset-specific parameters, and limited domain generalization. Our approach addresses the limitations with two main contributions. First, to resolve label heterogeneity and dataset-specific parameters, we employ nonparametric prototypes to unify diverse keypoint annotations across multiple datasets. Second, to address the limited multi-dataset supervision, we propose a cross-type self-supervision mechanism. The proposed method has demonstrated substantial improvements over existing MDT across a broad range of datasets, including human pose, animal pose, hand shape, and human shape estimation.

Limitations and future work. A limitation of our approach is that it requires at least a few-shot sample to learn prototypes, making zero-shot inference for unseen skeletons infeasible. Future work should explore extending our method for zero-shot human pose estimation. Future work should also investigate adapting the approach to 3D domains e.g. using axis-angle rotation representations, to facilitate representation learning on 3D manifolds.

Acknowledgments. This work was supported by the National Research Foundation of Korea (NRF) grant (No. 2021R1A2C2012195) and by the Institute of Information & communications Technology Planning & Evaluation (IITP) grants No. RS-2019-II191906 (AI Graduate School Program, POSTECH), No. RS-2020-II201336 (AI Grad-

uate School Program, UNIST), and RS-2022-II220290, funded by the Korea government (MSIT).

References

- [1] Mykhaylo Andriluka, Leonid Pishchulin, Peter Gehler, and Bernt Schiele. 2D human pose estimation: New benchmark and state of the art analysis. In *IEEE/CVF Conference on Computer Vision and Pattern Recognition (CVPR)*, 2014. 1, 5
- [2] Mykhaylo Andriluka, Umar Iqbal, Eldar Insafutdinov, Leonid Pishchulin, Anton Milan, Juergen Gall, and Bernt Schiele. PoseTrack: A benchmark for human pose estimation and tracking. In *IEEE/CVF Conference on Computer Vision and Pattern Recognition (CVPR)*, pages 5167–5176, 2018. 2
- [3] Chaofan Chen, Oscar Li, Daniel Tao, Alina Barnett, Cynthia Rudin, and Jonathan K Su. This looks like that: Deep learning for interpretable image recognition. *Advances in Neural Information Processing Systems (NeurIPS)*, 32, 2019. 3
- [4] Yanbei Chen, Manchen Wang, Abhay Mittal, Zhenlin Xu, Paolo Favaro, Joseph Tighe, and Davide Modolo. ScaleDet: A scalable multi-dataset object detector. In *IEEE/CVF Conference on Computer Vision and Pattern Recognition (CVPR)*, pages 7288–7297, 2023. 2
- [5] Hongsuk Choi, Gyeongsik Moon, Joonkyu Park, and Kyoung Mu Lee. Learning to estimate robust 3D human mesh from in-the-wild crowded scenes. In *IEEE/CVF Conference on Computer Vision and Pattern Recognition (CVPR)*, 2022. 2
- [6] Yuanzheng Ci, Yizhou Wang, Meilin Chen, Shixiang Tang, Lei Bai, Feng Zhu, Rui Zhao, Fengwei Yu, Donglian Qi, and Wanli Ouyang. UniHCP: A unified model for human-centric perceptions. In *IEEE/CVF Conference on Computer Vision and Pattern Recognition (CVPR)*, pages 17840–17852, 2023. 1, 2
- [7] Mickael Cormier, Aris Clepe, Andreas Specker, and Jürgen Beyerer. Where are we with human pose estimation in real-world surveillance? In *IEEE/CVF Winter Conference on Applications of Computer Vision*, pages 591–601, 2022. 1
- [8] Anurag Das, Yongqin Xian, Dengxin Dai, and Bernt Schiele. Weakly-supervised domain adaptive semantic segmentation with prototypical contrastive learning. In *IEEE/CVF Conference on Computer Vision and Pattern Recognition (CVPR)*, pages 15434–15443, 2023. 3
- [9] Jon Donnelly, Alina Jade Barnett, and Chaofan Chen. Deformable protopnet: An interpretable image classifier using deformable prototypes. In *IEEE/CVF Conference on Computer Vision and Pattern Recognition (CVPR)*, pages 10265–10275, 2022. 3
- [10] Ye Du, Zehua Fu, Qingjie Liu, and Yunhong Wang. Weakly supervised semantic segmentation by pixel-to-prototype contrast. In *IEEE/CVF Conference on Computer Vision and Pattern Recognition (CVPR)*, pages 4320–4329, 2022. 3
- [11] Stefan Elfving, Eiji Uchibe, and Kenji Doya. Sigmoid-weighted linear units for neural network function approximation in reinforcement learning. *Neural networks*, 107:3–11, 2018. 12
- [12] Zigang Geng, Chunyu Wang, Yixuan Wei, Ze Liu, Houqiang Li, and Han Hu. Human pose as compositional tokens. In *IEEE/CVF Conference on Computer Vision and Pattern Recognition (CVPR)*, 2023. 6, 13
- [13] Vladimir Guzov, Aymen Mir, Torsten Sattler, and Gerard Pons-Moll. Human POSEitioning System (HPS): 3D human pose estimation and self-localization in large scenes from body-mounted sensors. In *IEEE/CVF Conference on Computer Vision and Pattern Recognition (CVPR)*, pages 4318–4329, 2021. 1
- [14] Or Hirschhorn and Shai Avidan. A graph-based approach for category-agnostic pose estimation, 2024. 2
- [15] Wei Jiang, Kwang Moo Yi, Golnoosh Samei, Oncel Tuzel, and Anurag Ranjan. NeuMan: Neural human radiance field from a single video. In *European Conference on Computer Vision (ECCV)*, 2022. 1
- [16] Roy Kapon, Guy Tevet, Daniel Cohen-Or, and Amit H Bermano. MAS: Multi-view ancestral sampling for 3D motion generation using 2D diffusion. In *IEEE/CVF Conference on Computer Vision and Pattern Recognition (CVPR)*, pages 1965–1974, 2024. 1
- [17] Rawal Khirodkar, Timur Bagautdinov, Julieta Martinez, Su Zhaoen, Austin James, Peter Selednik, Stuart Anderson, and Shunsuke Saito. Sapiens: Foundation for human vision models. *arXiv preprint arXiv:2408.12569*, 2024. 2
- [18] Muhammed Kocabas, Chun-Hao P. Huang, Otmar Hilliges, and Michael J. Black. PARE: Part attention regressor for 3D human body estimation. In *IEEE/CVF International Conference on Computer Vision (ICCV)*, pages 11127–11137, 2021. 2
- [19] Alberto Lamas, Siham Tabik, Antonio Cano Montes, Francisco Pérez-Hernández, Jorge García, Roberto Olmos, and Francisco Herrera. Human pose estimation for mitigating false negatives in weapon detection in video-surveillance. *Neurocomputing*, 489:488–503, 2022. 1
- [20] John Lambert, Zhuang Liu, Ozan Sener, James Hays, and Vladlen Koltun. MSeg: A composite dataset for multi-domain semantic segmentation. In *IEEE/CVF Conference on Computer Vision and Pattern Recognition (CVPR)*, 2020. 2
- [21] Duy Tho Le, Chenhui Gou, Stavva Datta, Hengcan Shi, Ian Reid, Jianfei Cai, and Hamid Rezatofighi. JRDB-PanoTrack: An open-world panoptic segmentation and tracking robotic dataset in crowded human environments. In *IEEE/CVF Conference on Computer Vision and Pattern Recognition (CVPR)*, pages 22325–22334, 2024. 1
- [22] Yanjie Li, Sen Yang, Peidong Liu, Shoukui Zhang, Yunxiao Wang, Zhicheng Wang, Wankou Yang, and Shu-Tao Xia. SimCC: A simple coordinate classification perspective for human pose estimation. In *European Conference on Computer Vision (ECCV)*, pages 89–106. Springer, 2022. 6, 13
- [23] Jing Lin, Ailing Zeng, Shunlin Lu, Yuanhao Cai, Ruimao Zhang, Haoqian Wang, and Lei Zhang. Motion-X: A large-scale 3D expressive whole-body human motion dataset. *Advances in Neural Information Processing Systems (NeurIPS)*, 2023. 1
- [24] Tsung-Yi Lin, Michael Maire, Serge Belongie, James Hays, Pietro Perona, Deva Ramanan, Piotr Dollár, and C Lawrence

- Zitnick. Microsoft COCO: Common objects in context. In *European Conference on Computer Vision (ECCV)*, pages 740–755. Springer, 2014. 1, 5
- [25] Sun-Ao Liu, Yiheng Zhang, Zhaofan Qiu, Hongtao Xie, Yongdong Zhang, and Ting Yao. Learning orthogonal prototypes for generalized few-shot semantic segmentation. In *IEEE/CVF Conference on Computer Vision and Pattern Recognition (CVPR)*, 2023. 3
- [26] Xian Liu, Xiaohang Zhan, Jiayang Tang, Ying Shan, Gang Zeng, Dahua Lin, Xihui Liu, and Ziwei Liu. HumanGaussian: Text-driven 3D human generation with gaussian splatting. In *IEEE/CVF Conference on Computer Vision and Pattern Recognition (CVPR)*, pages 6646–6657, 2024. 1
- [27] Matthew Loper, Naureen Mahmood, Javier Romero, Gerard Pons-Moll, and Michael J. Black. SMPL: A skinned multi-person linear model. *ACM Trans. Graphics (Proc. SIGGRAPH Asia)*, 34(6):248:1–248:16, 2015. 6
- [28] Yawen Lu, Dongfang Liu, Qifan Wang, Cheng Han, Yiming Cui, Zhiwen Cao, Xueling Zhang, Yingjie Victor Chen, and Heng Fan. ProMotion: Prototypes as motion learners. In *IEEE/CVF Conference on Computer Vision and Pattern Recognition (CVPR)*, pages 28109–28119, 2024. 3
- [29] Gyeongsik Moon, Shou-I Yu, He Wen, Takaaki Shiratori, and Kyoung Mu Lee. InterHand2.6M: A dataset and baseline for 3D interacting hand pose estimation from a single rgb image. In *European Conference on Computer Vision (ECCV)*, 2020. 5
- [30] Gyeongsik Moon, Hongsuk Choi, and Kyoung Mu Lee. NeuralAnnot: Neural annotator for 3D human mesh training sets. In *Computer Vision and Pattern Recognition Workshop (CVPRW)*, 2022. 2
- [31] Gyeongsik Moon, Hongsuk Choi, Sanghyuk Chun, Jiyoung Lee, and Sangdoo Yun. Three Recipes for Better 3D Pseudo-GTs of 3D Human Mesh Estimation in the Wild. In *Computer Vision and Pattern Recognition Workshop (CVPRW)*, 2023. 2
- [32] Gyeongsik Moon, Takaaki Shiratori, and Shunsuke Saito. Expressive whole-body 3D gaussian avatar. In *European Conference on Computer Vision (ECCV)*, 2024. 1
- [33] Haocong Rao and Chunyan Miao. TranSG: Transformer-based skeleton graph prototype contrastive learning with structure-trajectory prompted reconstruction for person re-identification. In *IEEE/CVF Conference on Computer Vision and Pattern Recognition (CVPR)*, pages 22118–22128, 2023. 3
- [34] Davis Rempe, Tolga Birdal, Aaron Hertzmann, Jimei Yang, Srinath Sridhar, and Leonidas J. Guibas. HuMoR: 3D human motion model for robust pose estimation. In *IEEE/CVF International Conference on Computer Vision (ICCV)*, 2021. 1
- [35] Javier Romero, Dimitrios Tzionas, and Michael J. Black. Embodied hands: Modeling and capturing hands and bodies together. *ACM Transactions on Graphics, (Proc. SIGGRAPH Asia)*, 36(6), 2017. 6
- [36] Karsten Roth, Oriol Vinyals, and Zeynep Akata. Non-isotropy regularization for proxy-based deep metric learning. In *IEEE/CVF Conference on Computer Vision and Pattern Recognition (CVPR)*, pages 7420–7430, 2022. 3
- [37] István Sárádi, Alexander Hermans, and Bastian Leibe. Learning 3D human pose estimation from dozens of datasets using a geometry-aware autoencoder to bridge between skeleton formats. In *IEEE/CVF Winter Conference on Applications of Computer Vision (WACV)*, 2023. 2
- [38] Samarth Sinha, Roman Shapovalov, Jeremy Reizenstein, Ignacio Rocco, Natalia Neverova, Andrea Vedaldi, and David Novotny. Common Pets in 3D: Dynamic new-view synthesis of real-life deformable categories. *IEEE/CVF Conference on Computer Vision and Pattern Recognition (CVPR)*, 2023. 15
- [39] Richard Sinkhorn and Paul Knopp. Concerning nonnegative matrices and doubly stochastic matrices. *Pacific Journal of Mathematics*, 21(2):343–348, 1967. 4
- [40] Jake Snell, Kevin Swersky, and Richard Zemel. Prototypical networks for few-shot learning. *Advances in Neural Information Processing Systems (NeurIPS)*, 30, 2017. 3
- [41] Markus D Solbach and John K Tsotsos. Vision-based fallen person detection for the elderly. In *IEEE/CVF international conference on computer vision workshops (ICCVW)*, pages 1433–1442, 2017. 1
- [42] Ke Sun, Bin Xiao, Dong Liu, and Jingdong Wang. Deep high-resolution representation learning for human pose estimation. In *IEEE/CVF Conference on Computer Vision and Pattern Recognition (CVPR)*, 2019. 5, 6, 13
- [43] Yu Sun, Qian Bao, Wu Liu, Yili Fu, Black Michael J., and Tao Mei. Monocular, one-stage, regression of multiple 3D people. In *IEEE/CVF International Conference on Computer Vision (ICCV)*, 2021. 2
- [44] Yu Sun, Wu Liu, Qian Bao, Yili Fu, Tao Mei, and Michael J Black. Putting people in their place: Monocular regression of 3D people in depth. In *IEEE/CVF Conference on Computer Vision and Pattern Recognition (CVPR)*, 2022. 2
- [45] Denis Tome, Patrick Peluse, Lourdes Agapito, and Hernan Badino. xR-EgoPose: Egocentric 3D human pose from an hmd camera. In *IEEE/CVF International Conference on Computer Vision (ICCV)*, pages 7728–7738, 2019. 1
- [46] Edward Vendrow, Duy Tho Le, Jianfei Cai, and Hamid Rezaatoughi. JRDB-Pose: A large-scale dataset for multi-person pose estimation and tracking. In *IEEE/CVF Conference on Computer Vision and Pattern Recognition (CVPR)*, 2023. 1
- [47] Timo von Marcard, Roberto Henschel, Michael Black, Bodo Rosenhahn, and Gerard Pons-Moll. Recovering accurate 3D human pose in the wild using imus and a moving camera. In *European Conference on Computer Vision (ECCV)*, 2018. 5
- [48] Chong Wang, Yuyuan Liu, Yuanhong Chen, Fengbei Liu, Yu Tian, Davis McCarthy, Helen Frazer, and Gustavo Carneiro. Learning support and trivial prototypes for interpretable image classification. In *IEEE/CVF International Conference on Computer Vision (ICCV)*, pages 2062–2072, 2023. 3
- [49] Jian Wang, Diogo Luvizon, Weipeng Xu, Lingjie Liu, Kripasindhu Sarkar, and Christian Theobalt. Scene-aware ego-centric 3D human pose estimation. In *IEEE/CVF Conference on Computer Vision and Pattern Recognition (CVPR)*, pages 13031–13040, 2023. 1
- [50] Xudong Wang, Zhaowei Cai, Dashan Gao, and Nuno Vasconcelos. Towards universal object detection by domain at-

- tention. In *IEEE/CVF Conference on Computer Vision and Pattern Recognition (CVPR)*, pages 7289–7298, 2019. 2
- [51] Zhongdao Wang, Hengshuang Zhao, Ya-Li Li, Shengjin Wang, Philip Torr, and Luca Bertinetto. Do different tracking tasks require different appearance models? *Advances in Neural Information Processing Systems (NeurIPS)*, 34:726–738, 2021. 2
- [52] Jiahong Wu, He Zheng, Bo Zhao, Yixin Li, Baoming Yan, Rui Liang, Wenjia Wang, Shipei Zhou, Guosen Lin, Yanwei Fu, et al. AI Challenger: A large-scale dataset for going deeper in image understanding. *arXiv preprint arXiv:1711.06475*, 2017. 5
- [53] Bin Xiao, Haiping Wu, and Yichen Wei. Simple baselines for human pose estimation and tracking. In *European Conference on Computer Vision (ECCV)*, pages 466–481, 2018. 13
- [54] Hang Xu, Linpu Fang, Xiaodan Liang, Wenxiong Kang, and Zhenguo Li. Universal-RCNN: Universal object detector via transferable graph r-cnn. In *AAAI Conference on Artificial Intelligence (AAAI)*, pages 12492–12499, 2020. 2
- [55] Lumin Xu, Sheng Jin, Wang Zeng, Wentao Liu, Chen Qian, Wanli Ouyang, Ping Luo, and Xiaogang Wang. Pose for everything: Towards category-agnostic pose estimation. In *European Conference on Computer Vision (ECCV)*, pages 398–416. Springer, 2022. 2
- [56] Yufei Xu, Jing Zhang, Qiming Zhang, and Dacheng Tao. ViTPose++: Vision transformer for generic body pose estimation. *IEEE Transactions on Pattern Analysis and Machine Intelligence*, 2023. 2, 5, 12
- [57] Yuan Xu, Xiaoxuan Ma, Jiajun Su, Wentao Zhu, Yu Qiao, and Yizhou Wang. ScoreHypo: Probabilistic human mesh estimation with hypothesis scoring. In *IEEE/CVF Conference on Computer Vision and Pattern Recognition (CVPR)*, pages 979–989, 2024. 12
- [58] Di Yang, Yaohui Wang, Antitza Dantcheva, Lorenzo Garattoni, Gianpiero Francesca, and Francois Bremond. UNIK: A unified framework for real-world skeleton-based action recognition. *British Machine Vision Conference (BMVC)*, 2021. 2
- [59] Fengyuan Yang, Kerui Gu, and Angela Yao. KITRO: Refining human mesh by 2D clues and kinematic-tree rotation. In *IEEE/CVF Conference on Computer Vision and Pattern Recognition (CVPR)*, pages 1052–1061, 2024. 8
- [60] Yuxiang Yang, Junjie Yang, Yufei Xu, Jing Zhang, Long Lan, and Dacheng Tao. APT-36K: A large-scale benchmark for animal pose estimation and tracking. *Advances in Neural Information Processing Systems (NeurIPS)*, 35:17301–17313, 2022. 1, 5, 12
- [61] Sung Whan Yoon, Jun Seo, and Jaekyun Moon. TapNet: Neural network augmented with task-adaptive projection for few-shot learning. In *International conference on machine learning*, pages 7115–7123. PMLR, 2019. 3
- [62] Hang Yu, Yufei Xu, Jing Zhang, Wei Zhao, Ziyu Guan, and Dacheng Tao. AP-10K: A benchmark for animal pose estimation in the wild. In *Thirty-fifth Conference on Neural Information Processing Systems Datasets and Benchmarks Track (Round 2)*, 2021. 1, 5
- [63] Xinyi Yu, Xin Zhang, Chengjun Xu, and Linlin Ou. Human-robot collaborative interaction with human perception and action recognition. *Neurocomputing*, 563:126827, 2024. 1
- [64] Yuhui Yuan, Rao Fu, Lang Huang, Weihong Lin, Chao Zhang, Xilin Chen, and Jingdong Wang. HRFormer: High-resolution transformer for dense prediction. In *Advances in Neural Information Processing Systems (NeurIPS)*, 2021. 6
- [65] Baoquan Zhang, Xutao Li, Yunming Ye, Zhichao Huang, and Lisai Zhang. Prototype completion with primitive knowledge for few-shot learning. In *IEEE/CVF Conference on Computer Vision and Pattern Recognition (CVPR)*, pages 3754–3762, 2021. 3
- [66] Bo Zhang, Jiakang Yuan, Botian Shi, Tao Chen, Yikang Li, and Yu Qiao. Uni3D: A unified baseline for multi-dataset 3D object detection. In *IEEE/CVF Conference on Computer Vision and Pattern Recognition (CVPR)*, pages 9253–9262, 2023. 2
- [67] Song-Hai Zhang, Ruilong Li, Xin Dong, Paul Rosin, Zixi Cai, Xi Han, Dingcheng Yang, Haozhi Huang, and Shi-Min Hu. Pose2Seg: Detection free human instance segmentation. In *IEEE/CVF Conference on Computer Vision and Pattern Recognition (CVPR)*, pages 889–898, 2019. 13
- [68] Xiangyun Zhao, Samuel Schuster, Gaurav Sharma, Yi-Hsuan Tsai, Manmohan Chandraker, and Ying Wu. Object detection with a unified label space from multiple datasets. In *European Conference on Computer Vision (ECCV)*, pages 178–193. Springer, 2020. 2
- [69] Tianfei Zhou, Wenguan Wang, Ender Konukoglu, and Luc Van Gool. Rethinking Semantic Segmentation: A Prototype View. In *IEEE/CVF Conference on Computer Vision and Pattern Recognition (CVPR)*, pages 2582–2593, 2022. 3, 4, 12
- [70] Xingyi Zhou, Vladlen Koltun, and Philipp Krähenbühl. Simple multi-dataset detection. In *IEEE/CVF Conference on Computer Vision and Pattern Recognition (CVPR)*, pages 7571–7580, 2022. 2, 13

F	AP
32	77.1
64	77.1
128	77.1

Table 6. Impact of varying the embedding dimension F (mean AP on COCO validation set).

A. Supplemental material

In this supplementary material, we provide details on the keypoint embedding module (Appendix B) and experimental settings (Appendix C), as well as additional experimental results Appendix D).

B. Keypoint embedding module details

Our keypoint embedding module consists of two upsampling layers, one residual block, and two convolution layers. For the upsampling layers, we adopt the head design from ViTPose++ [56]. The residual block combines a standard 3×3 convolution with a skip connection, where we replace the ReLU activation with SiLU [11]. The final two convolution layers include a 3×3 convolution, batch normalization, SiLU activation, and a 1×1 output convolution. Although lightweight and simple, our embedding module effectively enhances multi-dataset training. We initialize the prototypes using a truncated normal distribution with a mean of 0, a standard deviation of 0.02, and a range of $[-2, 2]$, followed by L2-normalization across the embedding dimension.

C. Experimental setup

C.1. Hyperparameters

We set the embedding dimension to $F = 64$, the number of in-class prototypes to $M = 3$, and the total number of keypoints to $J = 214$. The output heatmap dimensions were set to a width of $W = 48$ and a height of $H = 64$. Following [69], we set $\kappa = 0.05$ for obtaining the target t_j . The prototype update momentum λ was set to 0.999. For the loss weights, we set $\alpha = 3.33 \times 10^{-6}$, $\beta = 1.25 \times 10^{-7}$, $\gamma = 1.25 \times 10^{-8}$, $\delta = 0.01$, and $\zeta = 0.001$. The impact of varying hyperparameter values (on the COCO validation set, measured in mean average precision; AP) is presented in Tabs. 6 to 8, demonstrating robust performance across different hyperparameter settings. The final hyperparameter values are highlighted in bold.

C.2. APT-36K preprocessing

For APT-36K [60], since official train, validation, and test splits are not provided, we partitioned the dataset using a 7:1:2 ratio following the guidelines of the original paper.

α		AP
3.33×10^{-6}		77.1
6.25×10^{-6}		77.1
1.25×10^{-5}		77.1
β	γ	AP
1.00×10^{-7}	1.00×10^{-8}	77.1
1.25×10^{-7}	1.25×10^{-8}	77.1
5.00×10^{-7}	5.00×10^{-8}	77.1
1.00×10^{-6}	1.00×10^{-7}	77.1

Table 7. Impact of varying the loss weight values α , β , and γ (mean AP on COCO validation set).

δ	AP	ζ	AP
5.0×10^{-3}	77.3	1.0×10^{-4}	77.3
1.0×10^{-2}	77.2	1.0×10^{-3}	77.2
5.0×10^{-2}	77.3	1.0×10^{-2}	77.3

Table 8. Impact of varying the loss weight values δ and ζ (mean AP on COCO validation set).

This resulted in approximately 24,900 images and 37,000 instances for training, 3,600 images and 5,400 instances for validation, and 6,900 images and 10,700 instances in testing. To ensure that videos in the validation and test sets do not appear in the training set, each video is assigned to a single split.

C.3. 3DPW

We use the processed annotations from ScoreHypo [57]. To obtain 2D keypoint annotations, we use the 2D projected 3D SMPL keypoints. We reformat the annotations to the COCO style and employ COCO-style evaluation metrics.

C.4. Training.

We trained our method on a system with four NVIDIA A100 GPUs or four NVIDIA A6000 GPUs using PyTorch 1.11 in an Ubuntu 20 environment. To enhance training efficiency, we also enabled automatic mixed precision with distributed training. We set the random seed value to 0 for all experiments to avoid randomness during training.

For learning rate scheduling, we start with an initial learning rate of 0.001 and reduce it by a factor of 0.1 at the 50th and 90th epochs. During the first 50 epochs, only the embedding module and prototypes are updated, while all other components remain frozen. At the start of the 50th epoch, we set the backbone and the multi-heads to be trainable and freeze the prototypes. We then apply the \mathcal{L}_{CSS} loss function (Eq. 8 in the main paper).

Method	AP	AP ⁵⁰	AP ⁷⁵	AP ^M	AP ^L	AR
ViTPose++-B	76.4	92.7	84.3	73.2	82.2	81.5
ViTPose++-H	78.5	93.4	86.2	75.3	84.4	83.4
Ours-B	76.6	92.6	84.4	73.4	82.4	81.7
Ours-H	78.6	93.3	86.2	75.3	84.4	83.5

Table 9. COCO test-dev evaluation results.

Method	Val	Test	Val (occ)	Test (occ)
ViTPose++-B	81.1	82.0	64.0	64.1
ViTPose++-H	85.7	86.8	72.6	72.9
Ours-B	82.2	83.1	66.3	66.2
Ours-H	86.0	87.0	73.2	73.7

Table 10. OCHuman evaluation results (measured in mean average precision; AP). Ground-truth bounding boxes were used for cropping.

Method	Average score
ViTPose++	68.2
+UniDet	68.9
Ours	70.6

Table 11. Performance of different MDT methods (average over six datasets).

Method	InterHand	3DPW
ViTPose++	86.2	81.7
Trn. scratch	86.1	56.8
AIC-trained	86.3	81.5
Ours	87.1	83.6

Table 12. Performance of domain transfer methods on the InterHand2.6M (AUC) and 3DPW (AP) datasets.

For transfer learning on InterHand2.6M, we follow ViTPose++ configurations. We train the model for 60 epochs with $5.0e-4$ initial learning rate. In the case of transfer learning on 3DPW, we train the model for 30 epochs with $1.0e-4$ initial learning rate. We train the prototypes for 30 epochs in InterHand2.6M, and 15 epochs in 3DPW.

D. Additional results

D.1. Quantitative results

Table 9 presents the pose estimation results on the COCO test-dev set. Following previous works [22, 42, 53], we cropped the input images based on detected bounding boxes. Our method outperforms the baseline ViTPose++ by

0.2 AP with the *Base* backbone and by 0.1 AP with the *Huge* backbone.

We also performed a downstream evaluation on unseen data using the OCHuman [67] dataset, which comprises 2,500 validation images and 2,231 test images, with no available training set. The results are presented in Tab. 10. Since OCHuman follows the COCO keypoint format, we used COCO-trained models for evaluation. Here, ‘(occ)’ denotes the evaluation of the occluded keypoints, following the protocol of [12]. Our method outperforms the baseline ViTPose++, particularly on the (occ) subsets, demonstrating its robustness to occlusion.

Pose estimation lacks a large, generic, high-quality dataset, which is a key motivation for our multi-dataset training (MDT) approach. As shown in Tab. 12, our method outperforms models trained from scratch or transferred from the *largest* single dataset (AIC) in domain transfer scenarios for pose estimation. Furthermore, compared to existing MDT problems (e.g., classification and detection), skeletal heterogeneity in pose estimation presents a unique challenge, making naïve dataset merging or multi-head supervision ineffective. Table 11 demonstrate this: Our method significantly outperforms conventional label merging approaches when applied to pose datasets such as UniDet [70].

D.2. Qualitative results

Figure 7 presents additional human pose estimation examples. In the first two rows, ViTPose++ struggles with accurate leg estimation and exhibits inconsistent keypoint predictions across different dataset skeletons. In contrast, our method accurately estimates the legs and maintains consistency across varying skeletons. In the bottom two rows, ViTPose++ incorrectly predicts the right and left foot at the same location, whereas our method correctly estimates the legs, except for AIC.

Figure 8 provides additional comparisons on the AP-10K animal dataset. For cattle (first two columns), ViTPose++ mislocalizes the left front leg in the APT-36K skeleton, while our method correctly identifies it. Similarly, in the last two columns (kangaroo), ViTPose++ confuses the right front leg with the left, an error our method successfully avoids.

Figure 9 and Figure 10 provide additional pose estimation examples of our algorithm on the InterHand2.6M and 3DPW datasets, respectively. Our method demonstrates strong generalization across hand and human shapes, even under various self-occlusion and external occlusion scenarios.

We visualize the prototypes constructed by our algorithm in Fig. 11, using those trained with the ViT-B backbone. The InterHand and 3DPW prototypes are separately trained during the domain transfer process, while others are

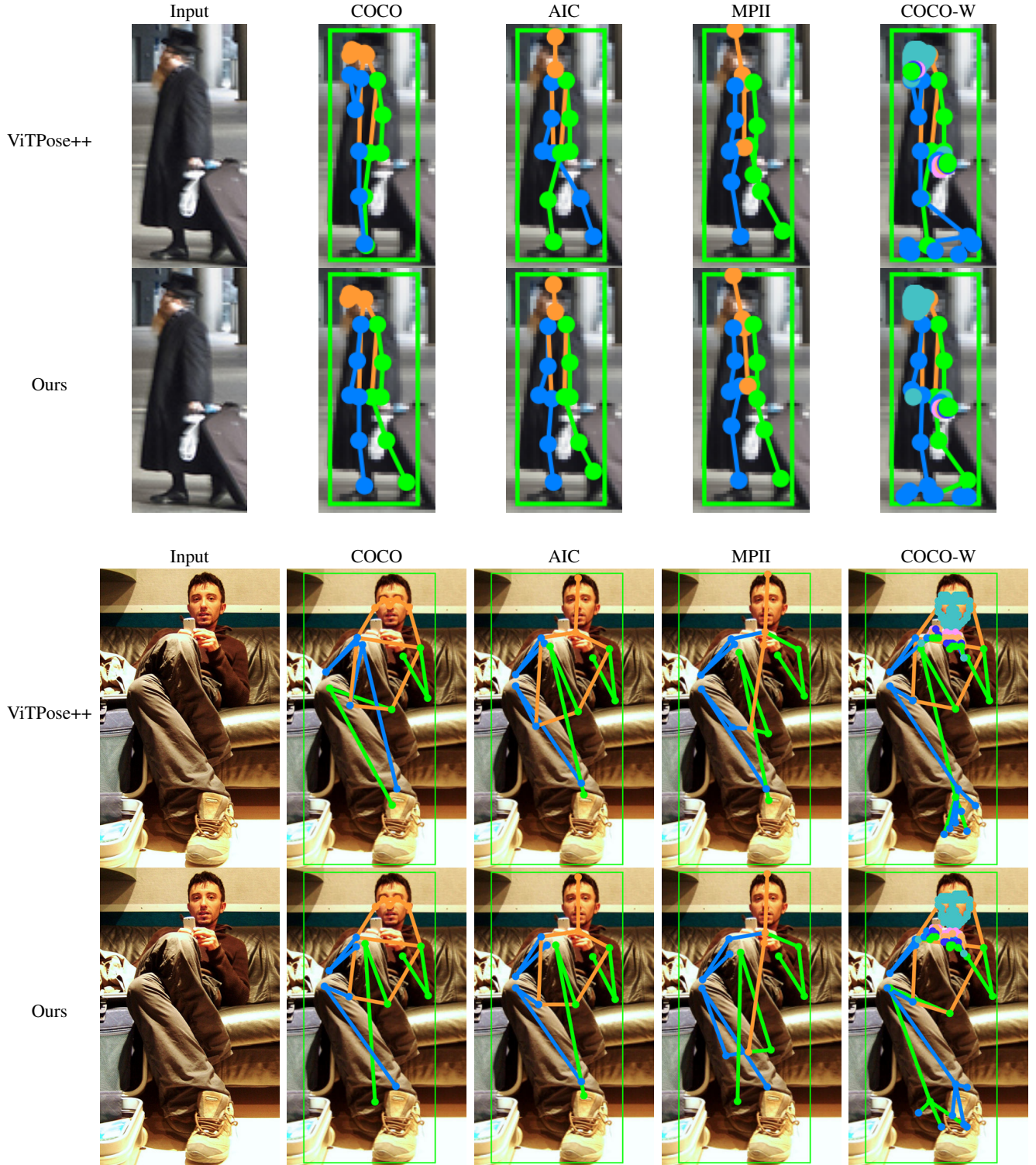


Figure 7. Pose estimation examples comparing ViTPose++ and our method.

jointly learned during MDT. The prototypes effectively capture the diversity of representations within the embedding space and successfully align similar keypoints across dif-

ferent datasets without compromising localization performance.

For example, in the upper red box in the figure, the

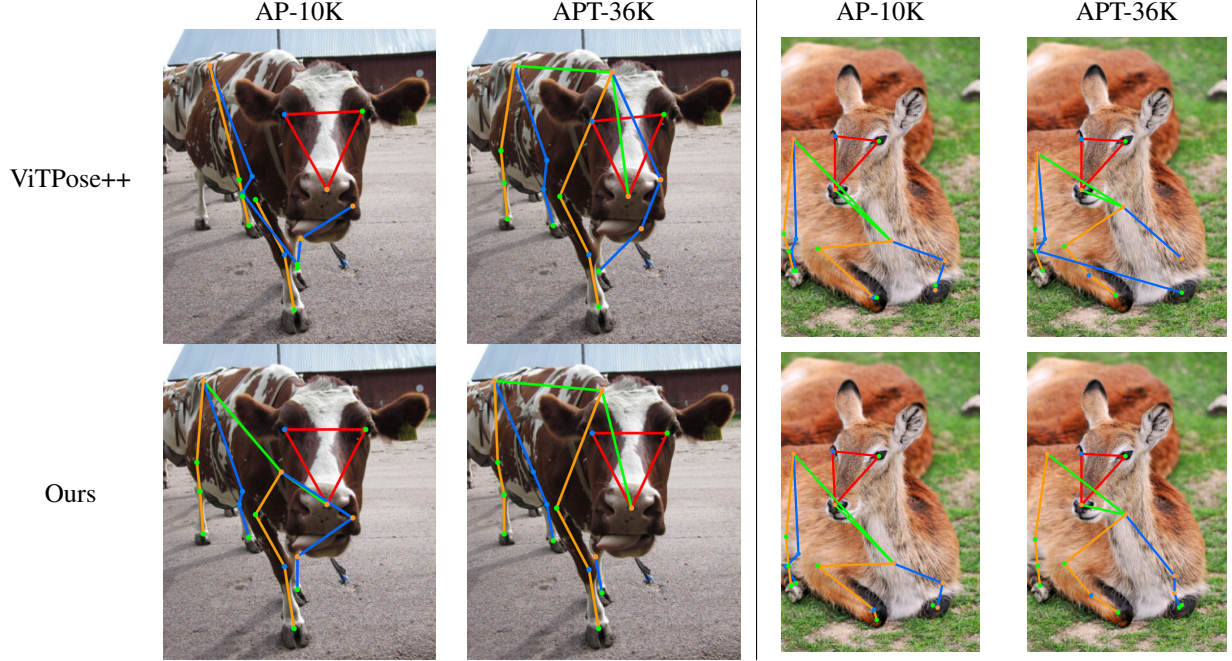


Figure 8. Pose estimation examples for animals using ViTPose++ and our method.

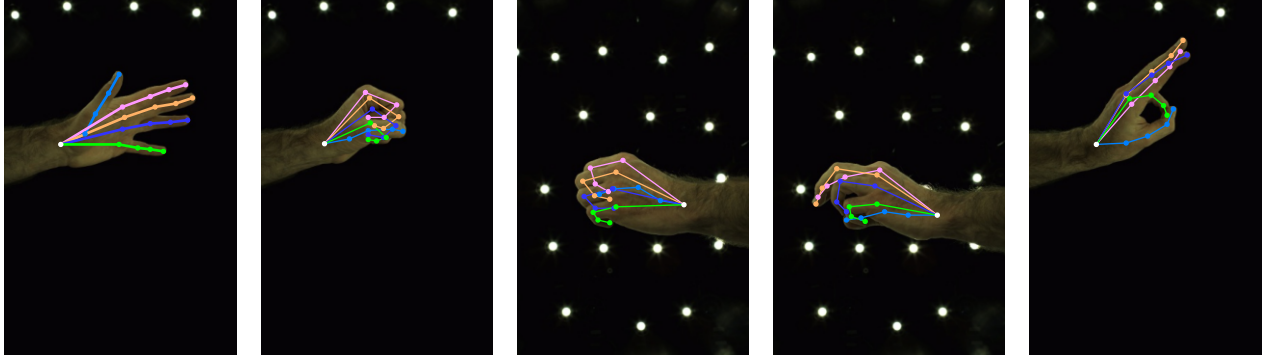


Figure 9. Pose estimation examples from our algorithm on the InterHand2.6M dataset.

COCO nose joint and the 3DPW jaw joint prototypes are closely aligned. Similarly, the lower red box contains a COCO left hip joint prototype and a 3DPW pelvis joint. As validated by domain transfer on InterHand and 3DPW, our learned embeddings effectively incorporate new skeletons without retraining of the embedding module.

D.3. Failure cases

In Fig. 12, we provide failure cases caused by unseen skeletons and poses. In (a–b), we show our COCO skeleton predictions on CrowdPose data. Since CrowdPose has a different skeletal structure than the training datasets, the predictions do not fully conform to its intended format, although the pose is reasonably well estimated in (a). Under strong occlusion (b), our method may also struggle to predict accu-

rate skeletons, as seen in the misplacement of the estimated left foot at the location of the right foot.

Similarly, (c–d) show our AP-10K skeleton predictions on a COP3D [38] example, where the pose deviates significantly from those observed during training (e.g. the cat’s head is tilted back, looking upward). In (d), our method fails to localize the cat’s eyes due to this challenging, unseen pose. Incorporating temporal information could improve robustness in such cases.

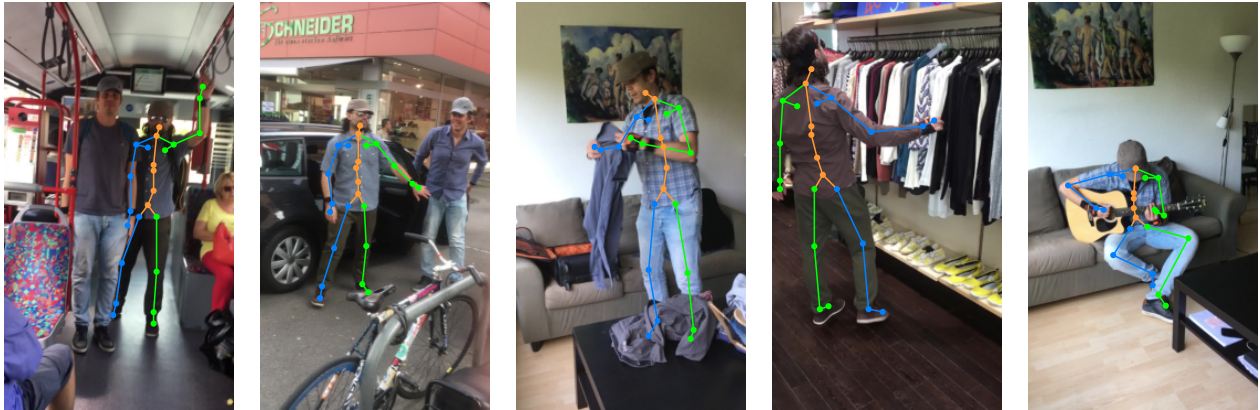


Figure 10. Pose estimation examples from our algorithm on the 3DPW dataset.

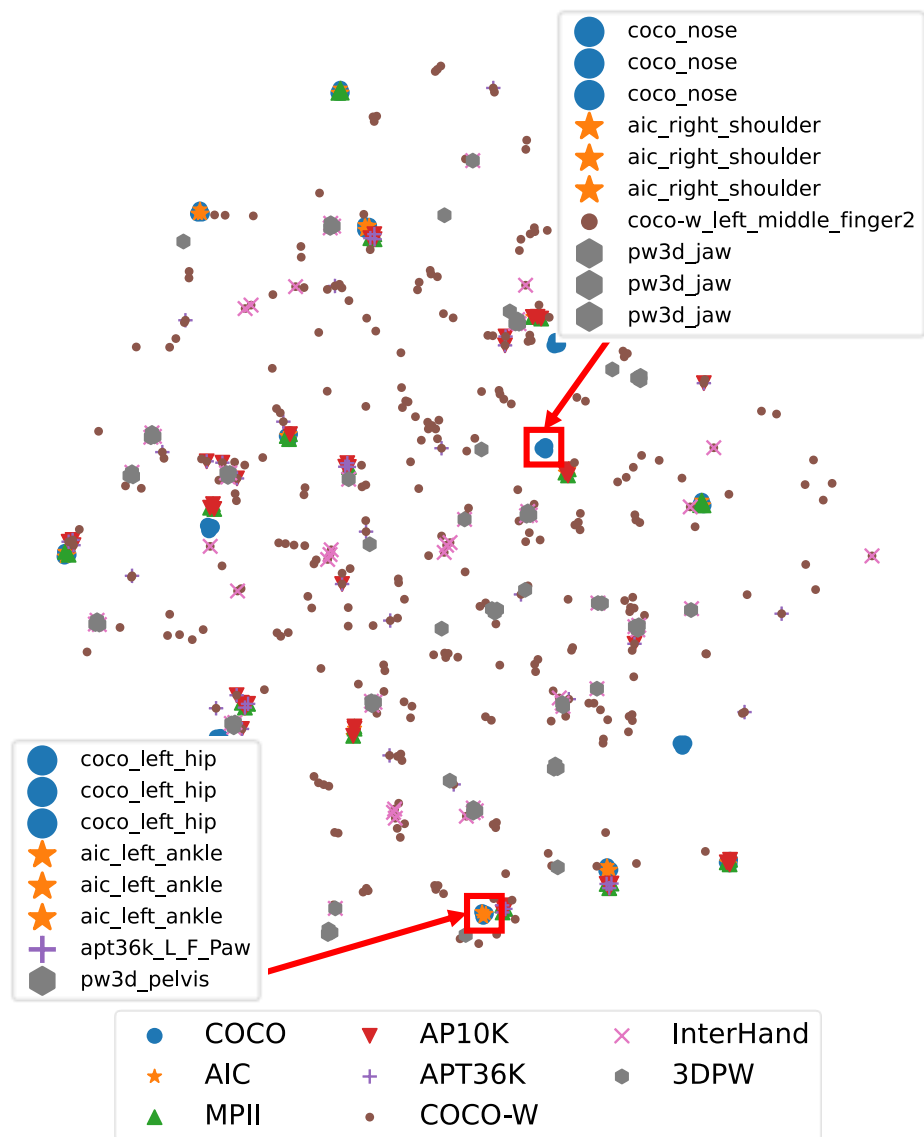


Figure 11. t-SNE visualization of the prototypes. Best viewed when zoom-in.

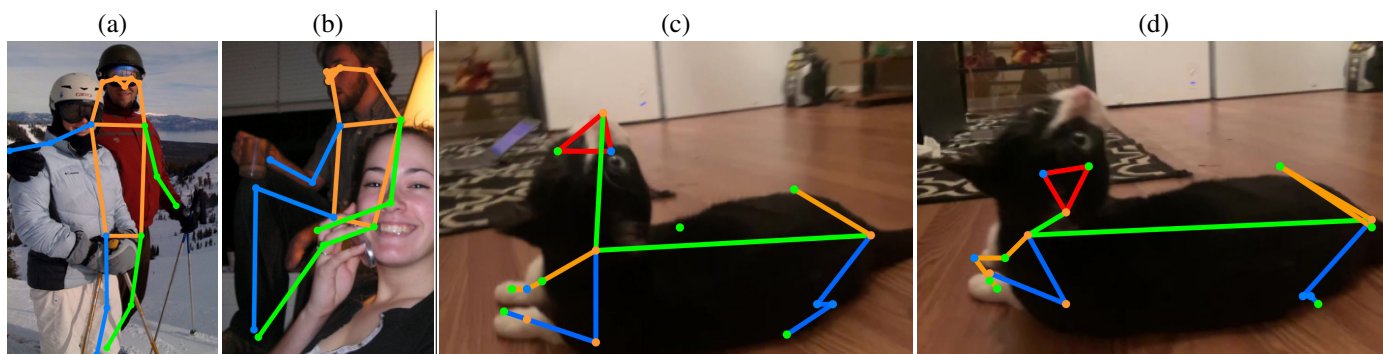


Figure 12. Example pose predictions: (a-b) CrowdPose predictions using the COCO skeleton; (c-d) COP3D predictions using the AP-10K skeleton.